DOI: 10.71762/d5yp-e678

Research Paper

Simulation and Thermo-Mechanical Analysis of AA6063-T5 in FSW by FEM

Younes Zarei[1], Ahmad Afsari[1], Seyed Mohammad Reza Nazemosadat[1*], Mohammad Mohammadi[1]

[1]Department of Mechanical Engineering, Faculty of Engineering, Shiraz Branch, Islamic Azad University, Shiraz, Iran

[*]Email of the Corresponding Author: smr.nazemosadat@iau.ac.ir; reza_nazemsadat@yahoo.com

Received: June 19, 2024; Accepted: August 25, 2024

Abstract

Temperature prediction is essential for assessing the state of stresses, strains, and material flow during friction stir welding (FSW). In this context, the thermal and mechanical behavior of the AA6063-T5 aluminum alloy was simulated in FSW. This research utilized the Finite Element Method (FEM) for thermal and mechanical simulations, employing Abaqus/Explicit software. The first simulation focused on the thermal model, implemented through coding in FORTRAN using the Schmidt-Hotel reference model, which investigates the temperature distribution of the alloy. The second simulation was mechanical in nature; it utilized the output results from the thermal simulation to examine the stresses resulting from the FSW process. The samples were made of the same material and were butt-jointed for the operation. A tool speed of 60 mm/min, a force of 4000 newtons, and a coefficient of friction of 0.4 were applied during this process. The parameters for thermal conductivity, specific heat, coefficient of expansion, and Young's modulus were defined as temperature-dependent. The results indicated that the temperature distribution diagram at a specific point along the welding path closely matched practical examples of the FSW process. The temperature distribution contours at the beginning, middle, and end of the welding path, as well as the temperature distribution across the cross-sectional surface of the weld in the middle of the piece, were consistent with the samples. Additionally, the diagram and contour of the longitudinal residual stress in the workpiece aligned well with the completed samples.

Keywords

FSW, FEM, Simulation, Thermal, Mechanical, AA6063-T5

1. Introduction

Friction stir welding is a solid-state joining process that uses a non-consumable tool to join two facing workpieces without melting the workpiece material [1]. The design of the tool is a critical factor, as a good tool can improve both the quality of the weld and the maximal possible welding speed. The tool material should be sufficiently strong, tough, and hard-wearing at the welding temperature. Further, it should have good oxidation resistance and a low thermal conductivity to minimize heat loss and thermal damage [2, 3]. An FSW tool is primarily composed of two vital components namely

shoulder and pin. The shoulder resting on the surface of the parts being welded, and generates the necessary frictional heat to soften the materials. Its design and size confine the material, ensuring it remains within the stirring area and undergoes a metallurgical phenomenon akin to extrusion. But the Pin, diving deep into the parts, the pin not only heats the material through a shearing effect but also guarantees material mixing. This is critical as parts often have an oxide layer. The pin's design and action ensure that materials close seamlessly behind the tool path, crushing the oxide for a flawless weld [4, 5]. Joints made with FSW are much stronger and more economical than traditional fusion welding techniques Furthermore, FSW improves weld quality, reduces defects, and lowers health hazards. The most significant parameters that contribute to the weld quality and affect the welded zone properties include the tool pin profile, rotational speed of the tool, and feed rate. The pin is designed to disrupt the faying or contacting surface of the workpiece, shear material in front of the tool, and move material behind the tool. Tool shoulder is designed to produce heat to the surface and subsurface regions of the welding material [6, 7]. There are several types of tool profiles such as cylindrical, threaded pin, and taper pin profile. However, each uses a different pin tool shape geometry and it affects the strength, macrostructure, and microstructure of the specimen [8].

Currently, the desire to offer this welding method by researchers in various applications of FSW has increased. However, empirical research imposes a very high rate of time and cost. In this situation, simulation and modeling methods lead us to a better, deeper, cheaper, and faster understanding of the process. Simulation of FSW is a challenging task due to various factors such as complex physical couplings between heat transfer and mechanics, significant strain rates and deformations in the stir zone (SZ) around the pin, and the need to track the material flow. Despite its attractiveness, the simulation of FSW is still a complex problem that requires careful consideration of multiple interrelated factors [9]. Numerical simulation of FSW includes the optimal selection of process parameters such as rotational and feed speeds [10, 11], tool penetration depth and tilt angle [12, 13], and the design of tool parameters such as tool shape and dimensions, shoulder and pin geometry [14-17]. Therefore, the simulation of FSW is a complex task, because it requires calculations for the interaction between different thermal and mechanical factors.

Nevertheless, advanced modeling methods have been developed that can effectively elucidate and predict fundamental aspects of the physics of FSW. These modeling methods cover a wide range of complexity, from basic conduction heat transfer models to more complex models that incorporate material flow, as well as fully coupled models that incorporate heat transfer and viscoplastic flow to predict temperature, strain, stress distributions, residual stress along with microstructure and texture distribution [18, 19]. FSW represents an advanced iteration of the conventional friction welding process and was originally conceived by the Welding Institute (TWI) in 1991. Since then, it has emerged as a leading metal joining method and is widely regarded as the most important development in the field over the past two decades [20 - 22].

Meyghani & Wu [23] have investigated the state of thermomechanical analysis of the FSW process to create guidelines for further investigation, fill existing research gaps, and expand the applications of FSW. Furthermore, the importance of key issues for thermo-mechanical analysis in this welding method is mentioned and then solid and fluid dynamics methods in modeling are explained and in addition, key issues in modeling are discussed. Thermomechanical properties of AA6061-T6 aluminum alloy during FSW are simulated based on COMSOL software using FEM. So, a conceptual

model was created to interpret the thermal and structural analysis and according to the obtained results, the temperature in the upper and lower levels increases with the increase of the axial force, but decreases along the line perpendicular to the welding direction. As the forward welding speed increases within the acceptable inducted temperature range of the workpiece, the overall temperature decreases, while the axial force and rotational speeds remain constant [24]. A FEM presented to simulate the thermomechanical behavior of aluminum alloy 6061 during FSW shows that the deformation caused by this welding method is of a two-step process. In addition to the stir action exerted by the rotating tool pin, the material near the surface of the stir zone also experienced secondary deformation by the pin shoulder edge after passing the welding tool. Both deformation stages were comparable in terms of temperature and strain, but the secondary deformation was primarily concentrated in the near-surface layer [25, 26].

In a survey, reviewed various methods and modeling methods for the analysis of FSW, including FEM, computational fluid dynamics, and other simulation methods. The advantages and limitations of each method are discussed and, in addition, it examines the effective variables that play an important role in the numerical modeling of the FSW [27].

In general, in friction welding, the heat required to create a weld is provided through mechanical energy caused by friction. Then, when the parts reach the state of plasticity due to the heat generated through friction, they are connected by applying pressure from both sides. The connection of metal with chemical compounds as well as different physical and mechanical properties causes many defects during the welding operation or even after. The difference can be between two different base metals as a result of which the composition of the weld metal will be different with all its components. This difference varies according to the joint design, welding process, and welding instructions. In this regard, the effect of these factors and also the heat treatment on the welding metal should be determined and should be accurately evaluated before production. The main goal of dissimilar metal welding is to create a connection that meets the requirements of the working conditions. This research focuses on aluminum AA6063-T5, analyzing its thermal and mechanical properties after simulation using Abaqus software in friction stir welding (FSW).

2. Materials and methods

In this research, first of all, it was necessary to obtain the required information about the welding operation to connect parts made of aluminum alloy AA6063-T5. For this purpose, FSW operation modeling was done. Abaqus software was used to simulate the process and finally, the numerical analysis of the parts welded behavior as well as the validation of the proposed model has been investigated to determine the behavior of the two mentioned aluminum sheets. The finite element method can be used to simulate and analyze material flow during FSW. As a result, the thermal and mechanical stresses on the workpiece and the welding tool can be analyzed. The effects of welding process parameters such as tool rotational speed, welding speed, tool tilt angle, welding tool depth, and tool shoulder diameter can be analyzed and optimized to increase the efficiency of the production process. Material characteristics of welded parts, such as hardness and grain size, can be analyzed to increase the quality of part production. Residual stress, strain, deformation, and estimation of temperatures in the welding area can be predicted by using FSW simulation by FEM. Heat generation, thermal, and thermomechanical analyses can also be performed on the welded parts to analyze the

temperature and strain distribution in the heat-affected zone. In addition, the welding operation of dissimilar metals can be analyzed using numerical simulation to increase the capabilities of the welding method in various industrial applications [28].

2.1 Process simulation by heat flux coding method

There are different methods such as the coding method, Couple-Euler-Lagrangian, etc., for simulating this process, but in this research, the heat flux coding method was used. Using the Schmidt-Hotel reference model, two surface and volumetric heat fluxes are applied to the tool and workpiece. Simulation in Abaqus software is done in two thermal and mechanical stages. In the first step, it is simulated by the heat flux of the heat distribution in the whole part by the coding method using the Schmidt-Hotel reference model. In this method, the tool is not physically modeled, but the characteristics of the tool are introduced to Abaqus software through coding in the FORTRAN language. In the following, the D-flux subroutine was used. In an indirect analysis, a heat flux that is a function of the spatial and temporal position of the tool and represents the heat input to the piece is applied to the workpiece. In the second step, the information is entered into Abaqus software as input in a mechanical analysis. Therefore, it is possible to examine the way of temperature distribution in AA6063-T5 aluminum alloy in FSW and also understand the resulting stresses in this alloy.

2.2 Coding method using Schmidt-Hotel reference model

Using the Schmidt model, the heat flux is divided into two parts. The first part of heat is applied to the shoulder of the tool and the second part of heat is applied to the bottom and around the pin of the tool. To apply the heat flux to the part, two surface and volume fluxes are used, which are done using relations 1 and 2 of these calculations [29].

$$Q_{sShoulder} = \frac{2\pi\omega\mu P}{3}\left(R^3{}_1 - R^3{}_2\right) \quad (1)$$

$$Q_{Pin} = Q_{Pinprofile} - Q_{Pinbottom} = 2\pi\mu\omega P R^2{}_2 H + \frac{2\pi\omega\mu P}{3} R^3{}_2 \quad (2)$$

In these relations:

$Q_{Shoulder}$: the heat produced by the tool shoulder, Q_{pin} is the total heat of the bottom and around the pin, $Q_{Pinprofile}$: heat around the tool pin and $Q_{Pinbottom}$ is the bottom heat of the tool pin.

ω: the angular velocity of the tool, μ: the coefficient of friction, and P: the force applied to the tool.

R_1: is the tool shoulder radius, R_2: is the pin radius and H is the height of the pin.

It is necessary to divide the first relation by the surface of the tool shoulder and the second relation by dividing the volume of the pin and using them in coding to apply the heat flux. It is obvious that the position of the tool changes at any moment with a constant acceleration. Therefore, the position of the surface and volume of the flux of the heat source changes at every moment. The coordinate relations including welding start point, welding speed, surface flux position, and volume of flux position are also changed in the coding that was introduced to the software. Likewise, the radius of the circle is introduced where the surface and volumetric heat fluxes should be applied to the software with relation 3 and 4 in coding.

$$R = \sqrt{X_f{}^2 + Z_f{}^2} \quad (3)$$

(ω) = rotational speed of the tool = 1000 rpm = 104.719 radians/second

$\mu = 0.4$, $P = 4$ KN, $R_1 = R_S = 10$mm, $R_2 = R_P = 3$mm, $H = Hp = 7.4$mm (4)

The tool pin radius (R_P), shoulder radius (R_S), pin height (Hp), and the origin point on the surface of the part must be specified in the coding. Using the relations (1) and (2), the values of the surface flux of the pin and volume of the shoulder of the tool should also be calculated and introduced to the software by coding.

FP = Flux Pin = 77541.3794640264 FS = Flux Shoulder =1194333.6205128 (5)

In the last stage of coding, the conditions for the software are determined and the written code is saved with the extension to be executed in the Abaqus software. To run, FORTRAN software must be linked with Abaqus software.

2.3. *Mechanical method*

As Figure 1 shows, in the FSW, the tool rotates toward the restrained part and goes down until the shoulder of the tool contacts the upper surface of the part. After a short time, the pin of the tool penetrates the space between the two parts to preheat them, then the forward movement of the tool starts and the tool moves along the connecting line and at the end of the path, the tool pulls up and comes out of the pieces [1].

After the penetration of the tool into the workpiece, produced heat by friction in three areas, (Figure 2). The first area (Q_1) is the frictional heat generated by the contact of the tool shoulder surface with the upper surface of the workpiece. The second area (Q_2) is the heat created by the contact of the pin body with the surface containing it inside the piece, and the third area (Q_3) is the frictional heat created by the lower surface of the pin and the workpiece, this thermal energy comes from the pin and shoulder of the tool.

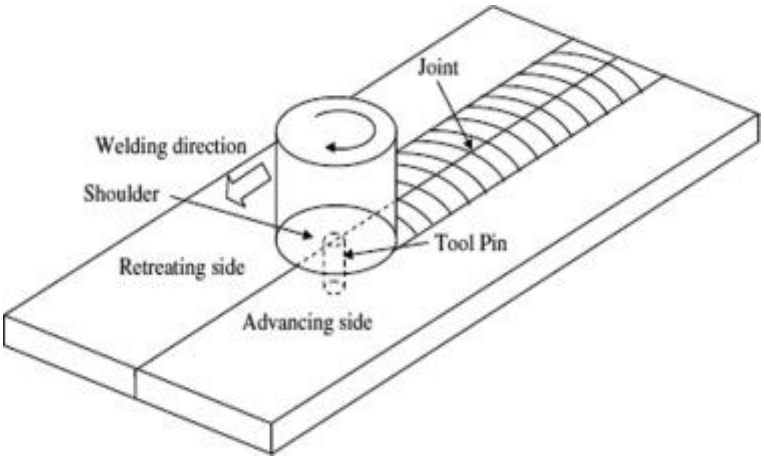

Figure 1. Schematic of FSW [1]

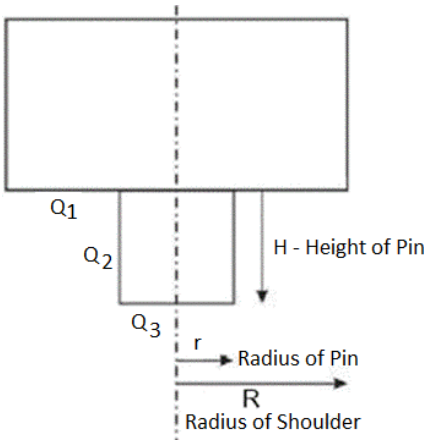

Figure 2. A simple tool without off-center [28]

Therefore, ignoring the plastic heat source according to Figure 3, the total frictional heat of the stir is equal to:

$$Q_{FSW} = Q_1 + Q_2 + Q_3 \quad (6)$$

Which can be considered the contribution of each according to the following relations:

$$Q_{FSW} = Q_{Shoulder} + Q_{Pin} \quad (7)$$

$$Q_{Shoulder} = Q_1 \quad (8)$$

$$Q_{Pin} = Q_1 + Q_2 \quad (9)$$

Based on the relationships of the Schmidt model, the frictional heat will be generated due to contact in three surfaces (Figure 3).

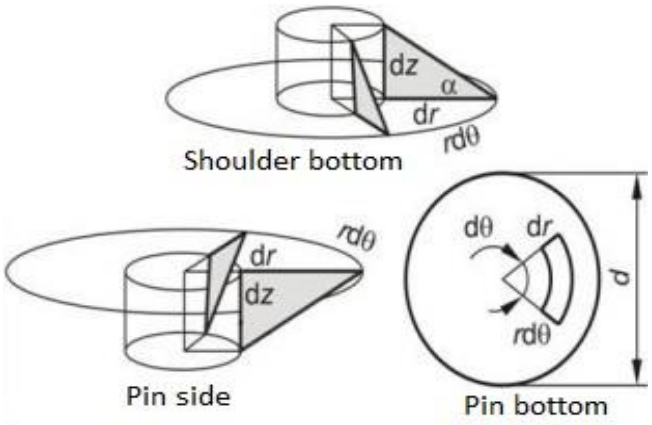

Figure 3. Triple zones that produce heat [8]

Using equation 10, it is possible to calculate the frictional heat produced in all three areas:

$$dQ = \omega r \tau_{Shear} dA \quad (10)$$

Were dA is contact surface differential. So, by using this relationship, the produced heat (Q_1) can be calculated as follows.

$$Q_1 = \int_0^{2\pi} \int_{R_{pin}}^{R_{Shoulder}} \omega\, \tau_{Shear}\, R^2(1 + tan\, \alpha) dr d\theta \quad (11)$$

$$Q_1 = \frac{2}{3}\, \pi\omega\tau_{Shear}(R^3{}_{Shoulder} - R^3{}_{Pin})(1 + tan\, \alpha) \quad (12)$$

In these relationships $R_{Shoulder}$ is the radius of the shoulder and R_{pin} is the radius of the pin of the tool. Likewise, the heat source Q_2 is the result of the frictional contact of the pin wall, which is calculated with the following relations.

$$Q_2 = \int_0^{2\pi} \int_0^{H_{Pin}} \omega\, \tau_{Shear}\, R^2{}_{Pin} dz d\theta \quad (13)$$

$$Q_2 = 2\, \pi\omega\tau_{Shear} R^2{}_{Pin} H_{Pin} \quad (14)$$

In these relationships, H_{pin} is the tool pin and Q_3 is the heat produced in the area of the bottom of the pin. These can be calculated in the form of the following relations.

$$Q_3 = \int_0^{2\pi} \int_0^{R_{Pin}} \omega\, \tau_{Shear}\, R^2 dr d\theta \quad (15)$$

$$Q_3 = \frac{2}{3}\, \pi\omega\tau_{Shear} R^3{}_{Pin} \quad (16)$$

If a tool with an off-center (e) is used, the frictional surfaces in the thermal triple zone will change (Figure 4).

By rewriting relations 3, 4, and 5, the frictional heat produced in the shoulder area is calculated from the following relation.

$$Q_1 = \int_0^{2\pi} \int_{R_{pin}+e}^{R_{Shoulder}} \omega\, \tau_{Shear}\, R^2(1 + tan\, \alpha) dr d\theta \quad (17)$$

$$Q_1 = \frac{2}{3}\, \pi\omega\tau_{Shear}(R^3{}_{Shoulder} - R^3{}_{Pin} + e)(1 + tan\, \alpha) \quad (18)$$

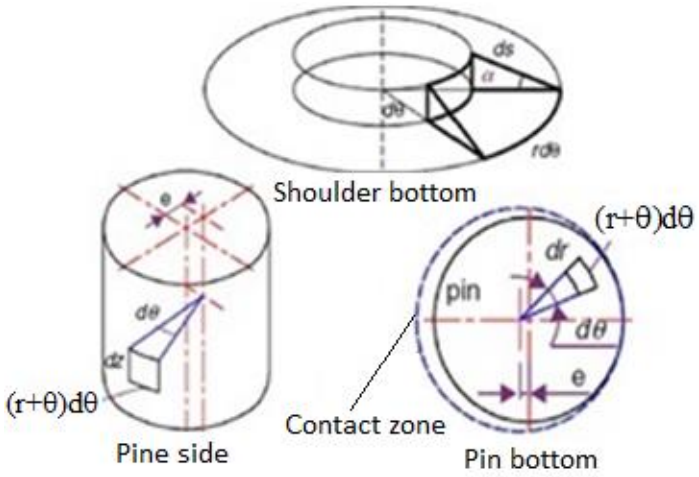

Figure 4. The three regions of heat are produced by the eccentric tool [2]

Likewise, the frictional heat produced in the area around the pin is rewritten as follows:

$$Q_2 = \int_0^{2\pi} \int_0^{H_{Pin}} \omega\, \tau_{Shear}\, (R_{Pin} + e)^2 dz d\theta \quad (19)$$

$$Q_2 = 2\,\pi\omega\tau_{Shear}(R_{Pin} + e)^2 H_{Pin} \quad (20)$$

Also, the relationship for the frictional heat area of the pin bottom will be equal to:

$$Q_3 = \int_0^{2\pi} \int_0^{R_{Pin}} \omega\, \tau_{Shear}\, (r + e)^2 dr d\theta \quad (21)$$

$$Q_3 = \frac{2}{3}\,\pi\omega\tau_{Shear}[(R_{Pin} + e)^3 - e] \quad (22)$$

The total heat produced by the friction for tools with an eccentric pin is also obtained from the following equation:

$$Q_{FSW} = \frac{2}{3}\pi\omega\tau_{Shear}[({R^3}_{Shoulder} - {R^3}_{Pin})(1 + tan\,\alpha) + ((R_{Pin} - e)^3 - e^3) + 3(R_{Pin} + e)^2 H_{Pin}]\ (16) \quad (23)$$

Except for τ_{Shear}, all parameters of the equation are constant. In some of the presented thermal models, the assumption of complete contact in all parts of the tool and workpiece is used, and the τ_{Shear}, is considered constant and a function of the yield stress of the material.

$$\tau_{Shear} = \frac{Q_{Yeild}}{\sqrt{3}} \quad (24)$$

Therefore, the total input heat has been calculated from the following equation, where (Q_{Yeild}) is the yield stress:

$$Q_{FSW} = \frac{2}{3}\pi\omega\frac{Q_{Yeild}}{\sqrt{3}}[({R^3}_{Shoulder} - {R^3}_{Pin})(1 + tan\,\alpha) + ((R_{Pin} - e)^3 - e^3) + 3(R_{Pin} + e)^2 H_{Pin}] \quad (25)$$

In some other thermal models, the complete sliding assumption has been used in three levels [18] and τ_{Shear}, is constant and a function of three parameters: friction coefficient (μ), total area of shoulder and bottom of the pin (A_{Total}) and the force applied to the tool (F_Z):

$$\tau_{Shear} = \mu\frac{F_z}{A_{Total}} \quad (26)$$

$$A_{Total} = \pi {R^2}_{Shoulder} \quad (27)$$

The total heat produced is calculated from this relationship:

$$Q_{FSW(Sliding)} = \frac{2}{3}\omega\mu\frac{F_z}{{R^2}_{Shoulder}}[({R^3}_{Shoulder} - {R^3}_{Pin})(1 + tan\,\alpha) + ((R_{Pin} - e)^3 - e^3) + 3(R_{Pin} + e)^2 H_{Pin}] \quad (28)$$

According to the experiments and studies, the friction conditions in the Q_1 and Q_2 friction areas are in the form of absolute adhesion due to the concentration of heat in these areas and the high-

temperature level close to the melting temperature of the material. But the main factor of heat production in the Q_3 zone will be in the contact area between the bottom of the pin and the workpiece, and due to the large distance from the shoulder, the temperature in this area is lower and will be in the form of sliding [28].

It should be mentioned that yield stress and friction coefficient are highly dependent on temperature changes, so it is necessary to define them as temperature-dependent. Therefore, assuming the dependence of two parameters yield stress and friction coefficient on temperature (T), shear stress is defined as follows.

$$\tau_{Shear}(Q_1) = \frac{\sigma_{Yeild}(T)}{\sqrt{3}} \quad (29)$$

$$\tau_{Shear}(Q_2) = \frac{\sigma_{Yeild}(T)}{\sqrt{3}} \quad (30)$$

$$\tau_{Shear}(Q_3) = \mu(T)\frac{F_z}{A_{Pin[} \quad (31)$$

Where A_{Pin} is the cross-sectional area of the tool pin. Considering the parameter $\boldsymbol{\lambda}$, the heat-generated equations of the triple zones are rewritten as below.

$$Q_1 = \frac{2}{3}\pi\lambda\omega\frac{Q_{Yeild}(T)}{\sqrt{3}}(R^3{}_{Shoulder} - (R_{Pin}+e)^3)(1+tan\,\alpha) \quad (32)$$

$$Q_1 = 2\pi\lambda\omega\frac{Q_{Yeild}(T)}{\sqrt{3}}(R_{Pin}+e)^2 H_{Pin} \quad (33)$$

$$Q_1 = \frac{2}{3}\pi\lambda\omega\mu(T)\frac{F_z}{A_{pin}}[(R_{Pin}+e)^3 - e^3] \quad (34)$$

Based on experimental studies, relatively large thermal cycles are created in the middle depths of the workpiece, and as a result, the temperature will increase significantly. Q_1 is considered a surface heat flux to the surface of the workpiece in the form of an enclosed area between the shoulder and the tool pin. Q_2 and Q_3, which are the heat sources created by the tool pin, are used as a factor creating a volumetric flux in the enclosed volume of the tool pin.

The final relations of two heat sources to apply two volume and surface heat fluxes on the workpiece will be as follows:

$$Q_{Pin} = 2\pi\lambda\omega\mu(T)\left[\frac{Q_{Yeild}(T)}{\sqrt{3}\mu(T)}(R_{Pin}+e)^2 + \frac{F_z}{A_{pin}H_{pin}}((R_{Pin}+e)^3 - e^3)\right] \quad (35)$$

$$Q_{Shoulder} = \frac{2}{3}\pi\lambda\omega\frac{Q_{Yeild}(T)}{\sqrt{3}}(R^3{}_{Shoulder} - (R_{Pin}+e)^3)(1+tan\alpha) \quad (36)$$

In these relations, all the parameters except yield stress and friction coefficient are constant. These two temperature-dependent parameters have been defined, which will ultimately lead to higher accuracy and precision of results in the simulation.

2.4 Thermal simulation using FORTRAN coding method in DFLUX subroutine format

In this research, to investigate the thermal and mechanical condition of AA6063-T5 aluminum alloy in FSW, two kinds of simulations have been performed using Abaqus Standard 2022 software. The first simulation was done using the FORTRAN coding method in the form of a DFLUX subroutine to consider the temperature distribution method in this alloy. Then, using the output of the first

simulation, the second simulation was done to check the resulting stresses in this process. Then, the results of the performed simulations are discussed.

This simulation is done using Schmidt's reference model [30]. In this method, the tool is not modeled geometrically, but its physical characteristics are applied, by coding in FORTRAN language, and in addition based on the relationships that exist in the reference model [30]. So the two calculated surface and volume heat fluxes related to the part are applied.

Instrument specifications

In this simulation, the tool is modeled simply and coded with the characteristics presented in Table 1.

Table 1. Tool specifications.

Tool pin radius	R_P = 3 mm = 0.003 m	welding time	T1 = 110 sec
Tool shoulder radius	R_S = 10 mm = 0.010 m	cooling time	T2 = 290 sec
Pin height	H = 4.7 mm = 0.0047 m	total time	T total = 400 sec
Tool rotational speed	V_X = 60 mm/min = 1 mm/sec = 0.001 m/secω	Start and end point from the edge	Start = 20 mm = 0.020 m, End = 20 mm = 0.020 m
Thermal flux of the shoulder	F_S = Flux Shoulder =1194333.62051282	Thermal flux of the pin	F_P = Flux Pin =3794640264.77541
Friction coefficient	μ = 0.4	Angular velocity	ω = 104.719 Rad/sec
Force on the tool	P = 4 KN = 4000 N	----	----

Part specifications

The parts are made of AA6063-T5 aluminum alloy with dimensions of 150 x 100 x 5 mm. It is worth mentioning that the samples are made of the same material and were designed as a butt joint to be introduced to the software. Due to having similar conditions in the entry of heat fluxes, it is modeled as a half part and the whole part will be observed and analyzed in the results section.

Steps of thermal simulation

In this section, model creation in the part module, assembly module, problem-solving steps in the stage module, interaction module, and meshing of the part in the mesh module are examined.

Creating a model in the Part module and determining the properties of the ingredients in the property module

Using the Abaqus software in the Part module, the modeling of the part with the dimensions of 150 ×100 × 5 mm was done (Figure 5). Then, thermal and mechanical properties according to Table 2 were introduced to Abaqus software in the property module (Figure 6).

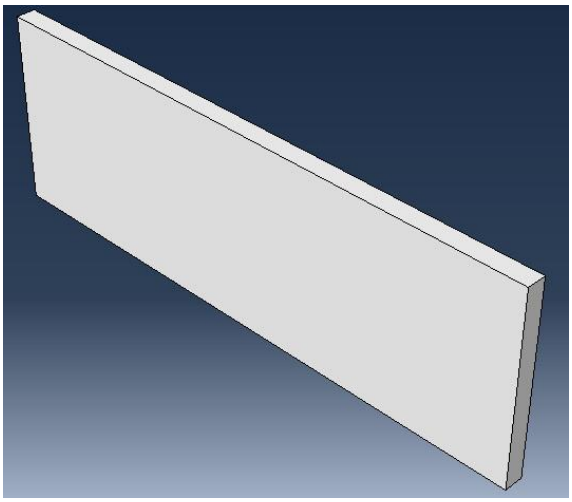

Figure 5. Compled the part model in the Part module

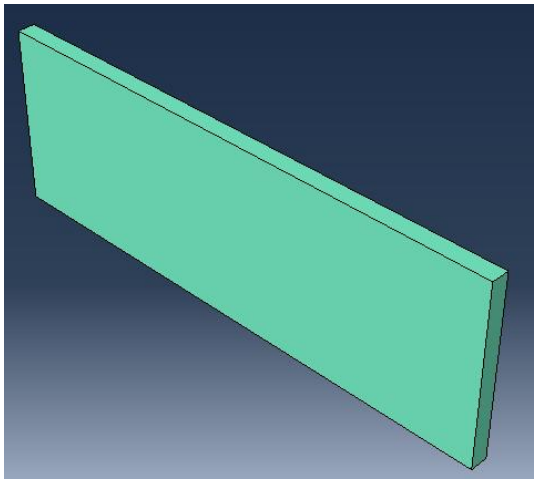

Figure 6. Assigned properties to the workpiece in the Property module

Table 2. Thermal and mechanical properties of aluminum alloy AA6063-T5.

temperature C°	density kgm^{-3}	Conductivity coefficient (W/m-K)	Specific Heat (J/g-°C)	Young's modulus (Pa)	Poisson's ratio	expansion coefficient
25	2680	191.75	913.25	688.3×10^{8}	0.33	2.18×10^{-5}
80	2669	195.6	935.8	653.9×10^{8}	0.33	2.38×10^{-5}
180	2652	202.6	976.8	519.2×10^{8}	0.33	2.47×10^{-5}
280	2634	209.6	1017.8	528.7×10^{8}	0.33	2.51×10^{-5}
380	2616	216.6	1058.8	466×10^{8}	0.33	2.55×10^{-5}
480	2598	223.6	1099.8	403.4×10^{8}	0.33	2.64×10^{-5}
Plastic properties						
Yield stress (Pa)		Ultimate stress (Pa)			Elongation (%)	
1.45×10^{8}		1.86×10^{8}			12	

Assembly Module

Initially, it is necessary to define and draw the model of the part and assign the required properties of the material for thermal simulation. The Assembly module of the Abaqus software is used and the workpiece is entered into the software independently (Figure 7-a). After the piece rotates by 90°, the origin point is moved according to Figure 7-b. The starting point of welding at the time of coding is defined as 20 mm after the origin point.

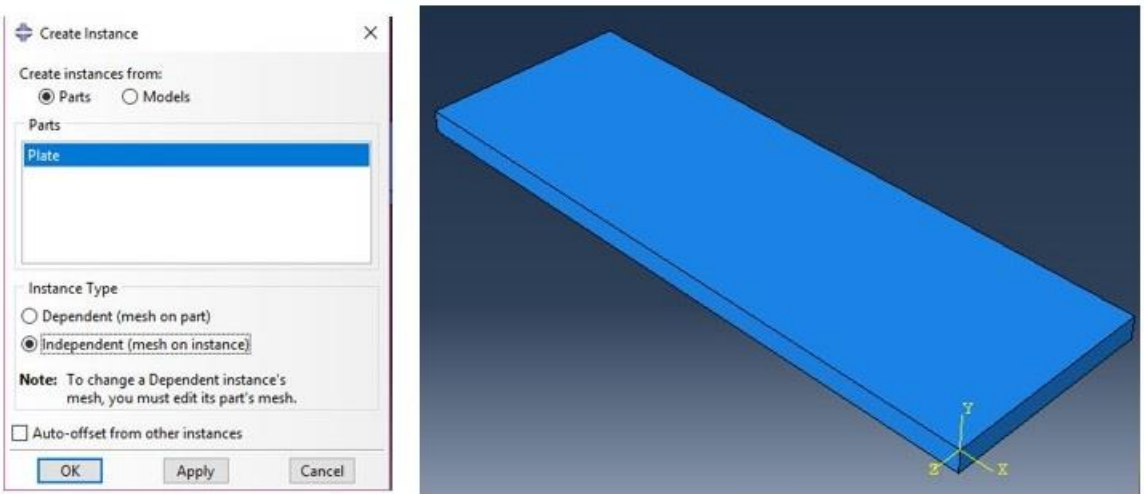

Figure 7. Assembling the workpiece in the Assembly module of Abaqus software

Problem-solving steps in the Step module

In this step, two steps of welding and cooling are used.

A- Welding step:

First, the welding step is defined as heat transfer, and the necessary settings are made in Abaqus software. Considering that the welding speed is 1 mm per second and the welding length is 110 mm, therefore the welding time was set to 110 seconds. The time of each increment is 0.25 seconds and its number is fixed. The maximum temperature of each increment is set to 100 °C.

B - Cooling step:

The cooling step was defined as heat transfer and its duration is 340 seconds.

C - Setting the output:

To see the results in the output of the thermal model, only field output is set. The software is asked to record each increment of the results. In this regard, the temperature of the nodes, the heat flux, and the temperature of the elements are adjusted.

D - Requesting the output of the results from the output menu of the Abaqus software:

Because of the temperature distribution obtained in these two steps and because the results of this model in the welding and cooling steps are used as input for the next model, which is a mechanical model. The distribution of stress, strain, etc. is obtained in the mechanical model, so for this purpose, it is necessary to appeal to the output of the results in this module.

Interaction module

In this module, radiation thermal boundary conditions and displacement boundary conditions are applied to the model. Stefan-Boltzmann relation is used for radiation boundary conditions. The ambient temperature is also defined.

A - Definition of absolute ambient temperature and Stefan-Boltzmann constant: Absolute zero temperature (-273) and Stefan –Boltzmann constant (5.67×10^{-8}) are entered into the software.

B - Definition of the heat transfer boundary condition on the bottom of the workpiece: During FSW, the bottom of the workpiece is in contact with other parts of the machine, so it is not modeled. In this regard, to consider the heat transfer from the workpiece to these parts, it is necessary to define a thermal boundary condition with a high coefficient such as 300 at a temperature of 25 degrees for the bottom. For this purpose, first, the thermal boundary condition of the bottom is named, then it is set in welding mode and the type of displacement boundary condition. Finally, the necessary settings are made by selecting the bottom of the part.

C - Definition of the boundary condition for heat transfer above and around the workpiece that is in contact with the surrounding air: In the following, it is necessary to create another heat transfer boundary condition for the upper parts as well as around the workpiece, which is in contact with the surrounding air. Similar to the previous step, after naming and making relevant settings, the top and surrounding parts are selected, except for the part inside it, and the value of displacement coefficient is set to 30 and the ambient temperature is set to 25 degrees Celsius: For this section, after naming and making relevant settings, similar to the previous steps, the upper and surrounding parts are selected, except for the bottom. The diffusion coefficient is set to 0.6 and the ambient temperature is set to 25°C.

Part meshing in the Mesh module

To have a proper meshing, the dimensions of the workpiece are considered in millimeters, and accordingly, the granularity is considered for the thickness of the piece of 5 elements and its length of 150 elements of a homogeneous type. For the width of the piece, which is modeled as a half piece, 25 non-homogeneous elements are considered so that towards the center of the piece, the elements become smaller and the heat distribution is done better (Figure 8). As we know, the number and size of elements are inversely proportional to each other. Therefore, the more the number of elements in the mesh created on geometry, the smaller the size of the elements [31,32]. In this research, after the mesh convergence operation, the number of suitable elements was 18750, and the number of suitable nodes 23556 of the type of linear heat transfer eight nodes DC3D8 were selected for the piece (Figure 9).

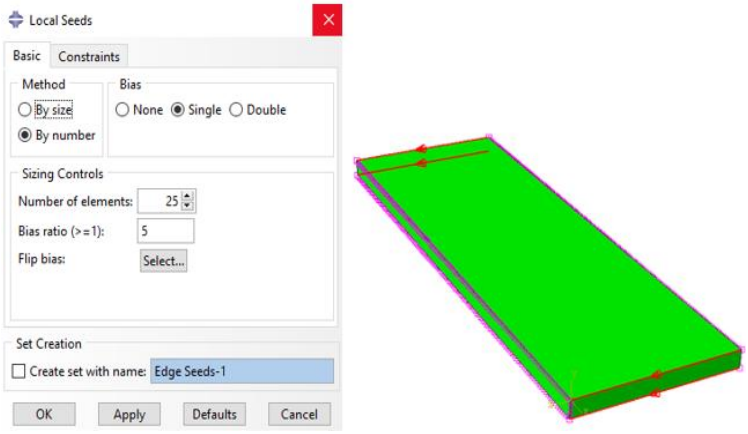

Figure 8. Non-homogeneous graining of piece width and its direction

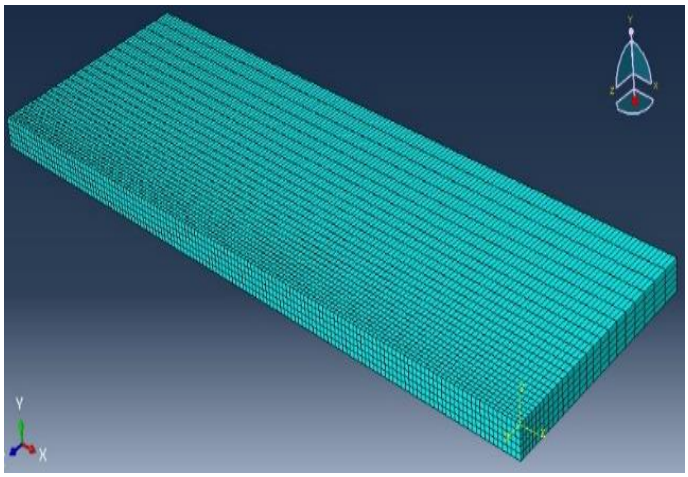

Figure 9. Completion of thermal model meshing

Heat flux coding with DFLUX subroutine in LOAD module

In this module, a surface heat flux and a volume flux have been applied. The heat of the tool shoulder is applied in a surface and the heat of the pin is applied in a volumetric manner. This work was done by writing code in FORTRAN language and then by linking it with Abaqus software. The surface heat flux is related to the shoulder of the tool and the module settings were made by selecting the surface of the workpiece (Figure 10).

By selecting the total volume of the workpiece and making its settings, the volumetric thermal flux of the pin to the workpiece was applied. So the desired flux was applied to the workpiece. Also, in this module, a boundary condition for the initial temperature of the workpiece was created. Schmidt's relations and coding in the subroutine theme are done by using FORTRAN language, and then problem solving was done in Abaqus software after linking (Figure 11).

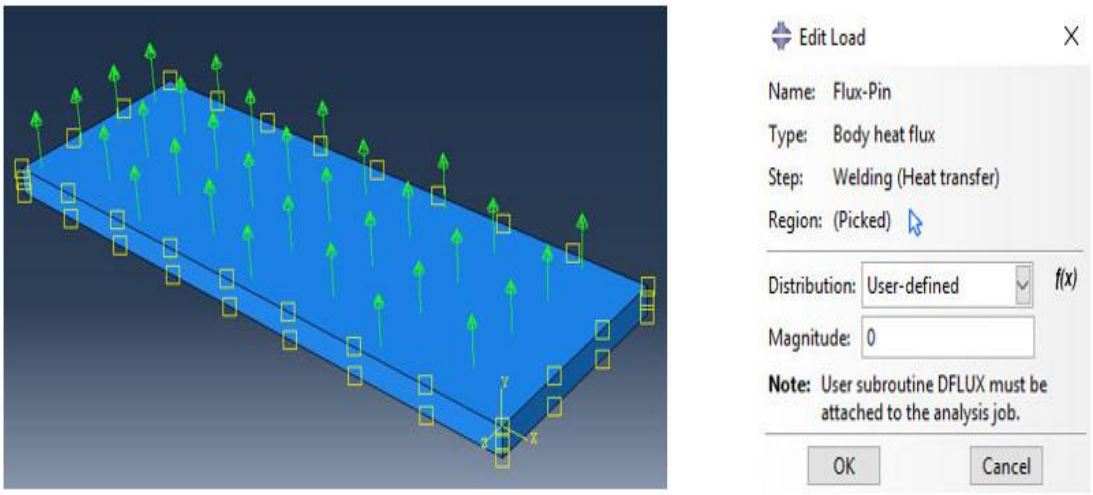

Figure 10. Adjusting the surface flux of the tool shoulder in User-defined mode and applying it to the surface of the workpiece

FSW.for - Notepad

File Edit Format View Help

```
      SUBROUTINE DFLUX(FLUX,SOL,KSTEP,KINC,TIME,NOEL,NPT,COORDS,
     1 JLTYP,TEMP,PRESS,SNAME)
C
      INCLUDE 'ABA_PARAM.INC'
C
      DIMENSION FLUX(2), TIME(2), COORDS(3)
      CHARACTER*80 SNAME
          T=Time(1)
        X=COORDS(1)
          Y=COORDS(2)
          Z=COORDS(3)
          X0=-0.02
          Y0=0
          Z0=0
          Vx=-0.001
          Vy=0
          Vz=0
          Xs=Vx*T+X0
          Ys=Vy*T+Y0
          Zs=Vz*T+Z0
          Xf=X-Xs
          Yf=Y-Ys
          Zf=Z-Zs
          R=SQRT(Xf**2+Zf**2)
          Rp=0.003
          Rs=0.01
          Hp=-0.0047
          FluxPin=3794640264.77541
          FluxShoulder=1194333.62051282
          IF(JLTYP.EQ.0 .AND. T.GE.0 .AND. R.LE.Rs .AND. R.GE.Rp)Then
          FLUX(1)=FluxShoulder
          ELSEIF(JLTYP.EQ.1 .AND. T.GE.0 .AND. R.LE.Rp .AND. Yf.GE.Hp)Then
          Flux(1)=FluxPin
          ENDIF
      RETURN
```

Figure 11. Coding in the subroutine theme in the FORTRAN language

Solving the problem in the job module

In this module, problem-solving is done by linking FORTRAN. Initially, a job was defined for this

task, and then the coded subroutine was introduced to the Abaqus software. Then the thermal solution of the problem was done and finally, due to its results, a mechanical model was created and its mechanical solution was also done.

2.5 Mechanical simulation

In mechanical simulation, thermal outputs are used in this simulation. The steps of mechanical simulation are the same as thermal simulation and include creating a model in the Part module, determining the properties of the constituent materials in the property module, assembling the part, setting the problem-solving steps, interaction module, loading module, meshing the model, setting the model outputs in Step module and job module.

3. Results and Discussion

In this section, the results of thermal simulation as well as the results of mechanical simulation are presented.

3.1 Thermal simulation results

The prediction of temperature in the FSW leads to the prediction of the state of stress, strain, and material flow during the process. The time history of the temperature of the workpiece is in simulation mode. The research model is shown in Figures 12 and 13, respectively, and the contour of temperature distribution on the surface of the workpiece (beginning-middle-end) is shown in Figure 14.

By comparing the temperature distribution diagram obtained from the simulation at one point of the welding path in Figure 13 and the results obtained from a research model, it can be seen that the results of this research are similar to the results obtained in this model although their alloys are not the same, but a good match has been achieved.

The temperature distribution contour in the workpiece after cooling (Figure 15) shows that the highest temperature is in the center of the piece and gradually decreases towards the sides. The temperature of the piece at the end of the cooling stage has almost reached the ambient temperature.

The distribution of the temperature of the weld cross-section area across the width of the workpiece can be seen so that the value of the temperature of the weld core is less in the lower part of the depth of the piece compared to the upper part of it. On the other hand, the heat distribution in the width section of the weld, changes by moving away from the weld core. It should be mentioned that these areas such as around the weld core and also the pin border will be predictable according to their temperature. The maximum temperature of the weld core is approximately 447.4°C, and it is near the melting point of the workpiece (Figure 16).

This is the same in the sample model even though they are made of two different aluminum alloys, so the accuracy of this modeling is confirmed (Figure 17).

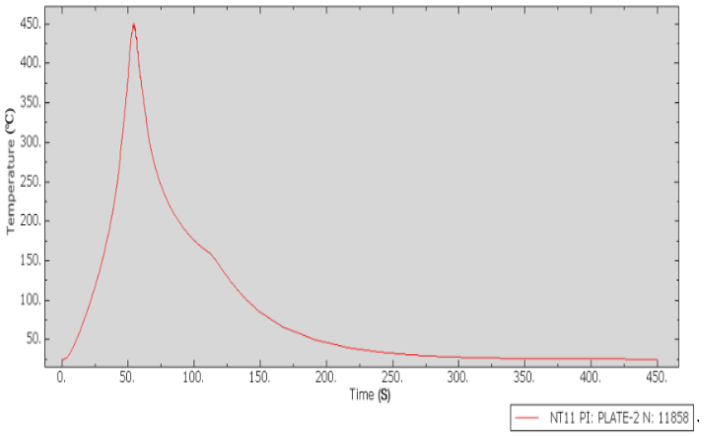

Figure 12. Temperature history of a point of the workpiece in thermal simulation

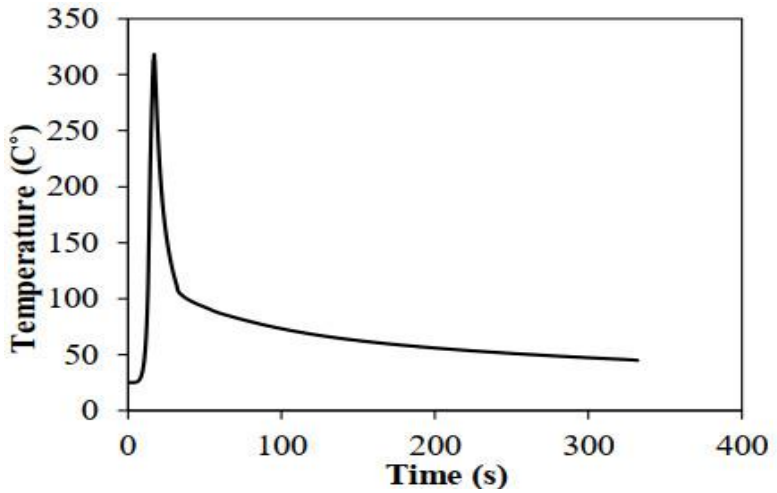

Figure 13. Time history chart of the temperature of one of the sample points of the model [1]

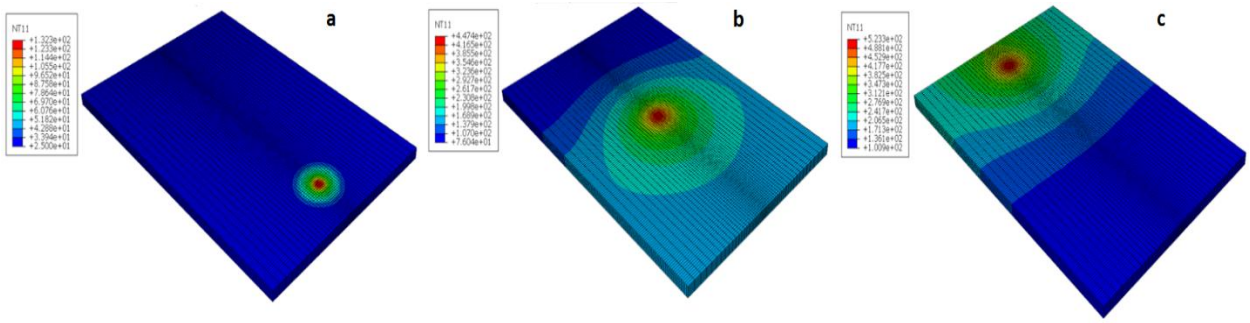

Figure 14 a) Contour of temperature distribution at the start point of welding b) Figure 14-b. Temperature distribution contour in the middle of the workpiece c) Contour of temperature distribution at the end point of welding

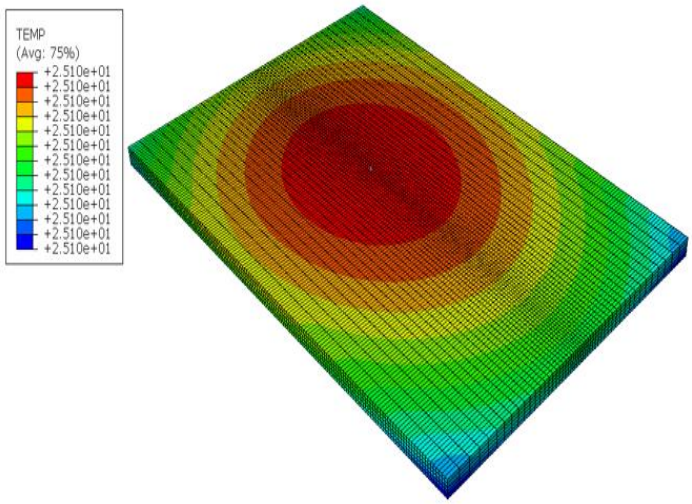

Figure 15. Contour of temperature distribution in the workpiece after cooling

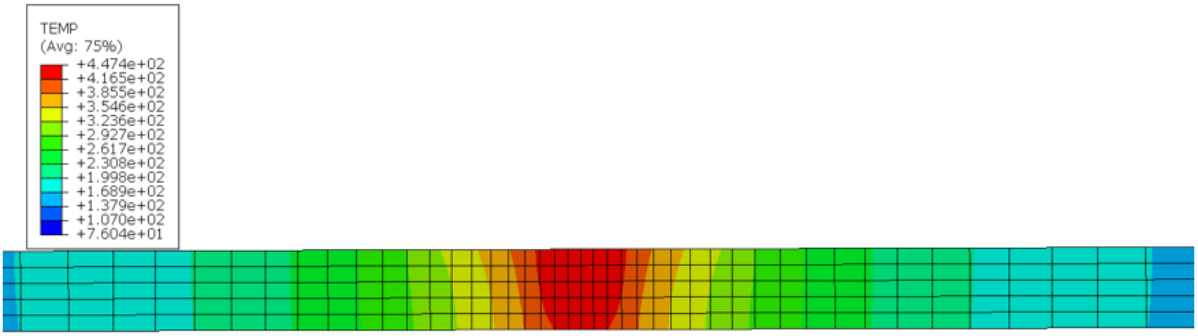

Figure 16. The temperature distribution of the cross-sectional surface of the weld in the middle of the part in the thermal simulation

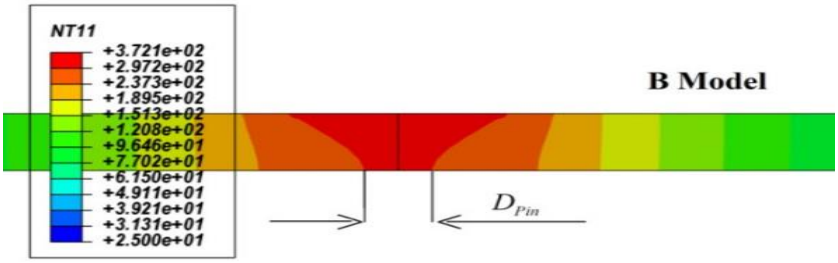

Figure 17. The contour of the heat distribution in a cross-section of the weld in the sample model [1]

3.2 Mechanical simulation results

Figure 18 shows the contour of the temperature distribution of the workpiece at 55 seconds, the maximum temperature of 447.5, which is almost near the temperature of the melting point of the part. Also, the contour of the temperature distribution of the workpiece in mechanical analysis shows the maximum temperature of the piece as in thermal analysis at about 447.5°C, and at the end of the welding operation, it reaches the ambient temperature of 25.08°C (Figure 19).

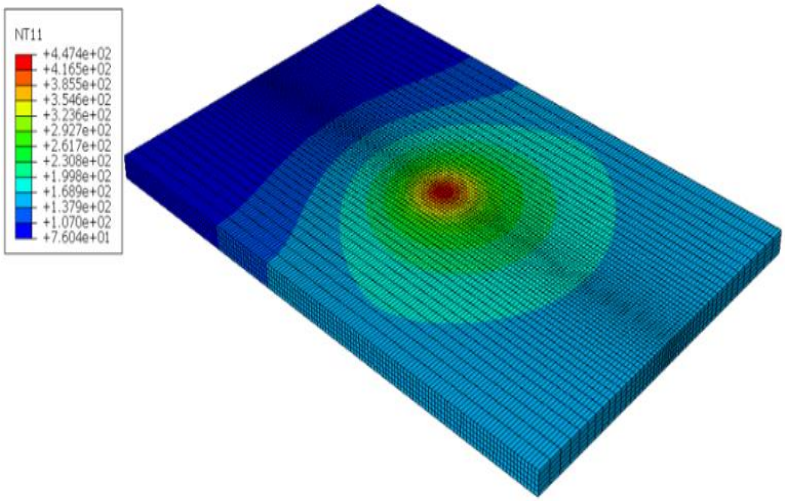

Figure18. The contour of the temperature distribution of the workpiece for 55 seconds

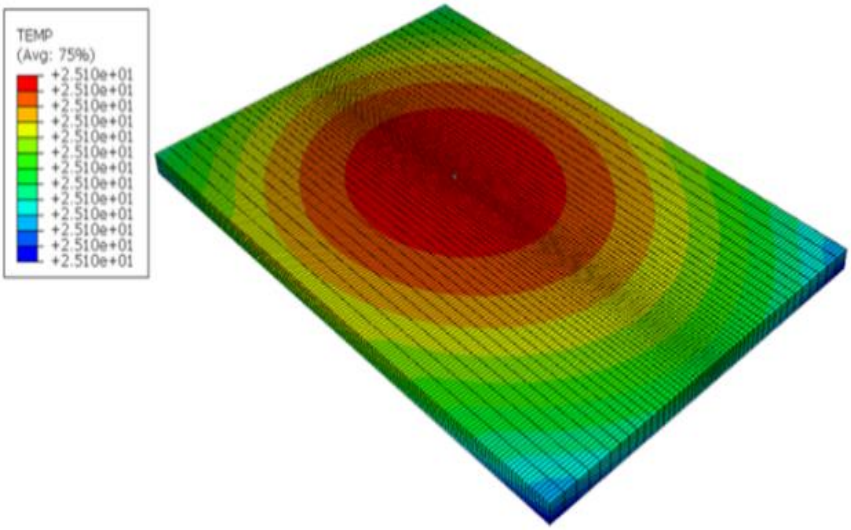

Figure 19. Workpiece temperature distribution contour in mechanical analysis

The longitudinal and transverse residual stress contours of the part show the maximum stresses of the part, which is shown in Figure 20 as an example of the longitudinal residual stress contour. The maximum value of the residual stress is equal to 1.546×10^8 MPa according to Figure 20. Figure 21 shows the contour of von Mises stress in the part, and different values of stresses at different points of the part. According to Figure 21, the maximum stress is equal to 1.688×10^8 MPa.

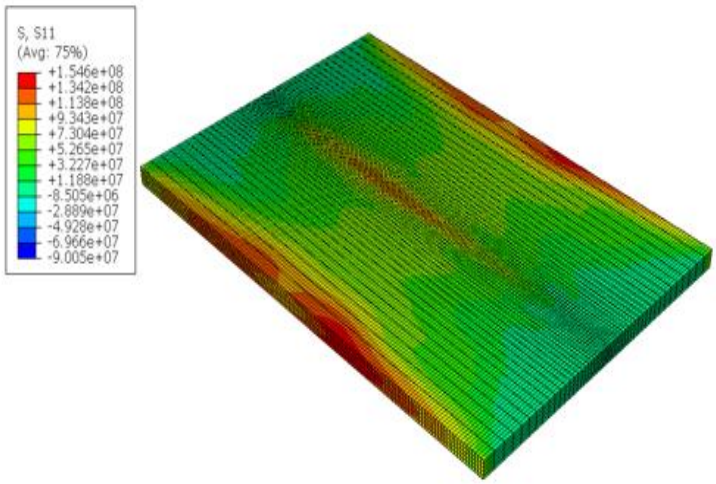

Figure20. Longitudinal residual stress contour of the workpiece

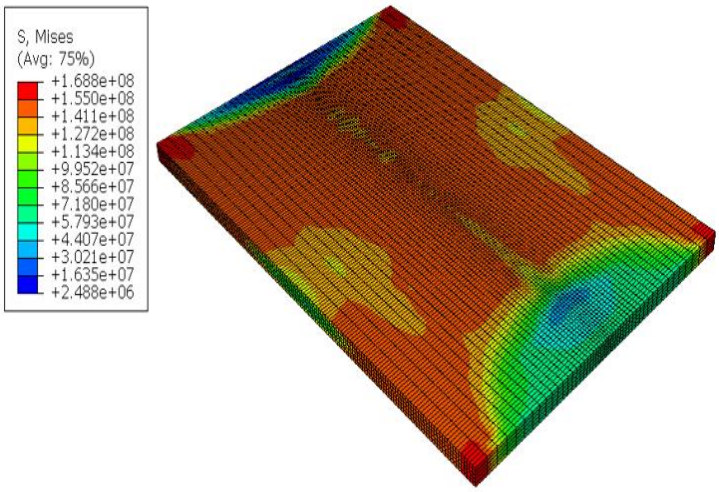

Figure 21. Von Mises stress contour in the workpiece

Figures 22 and 23 show longitudinal and transverse residual stress diagrams in one path of the piece. According to Figure 22, the highest longitudinal residual stress occurs in the middle of the welding line, and approaching the sides of the part, residual stresses are reduced. According to Figure 23, the lowest transverse residual stress is in the middle of the welding line and as it approaches the sides of the part, residual stresses increase.

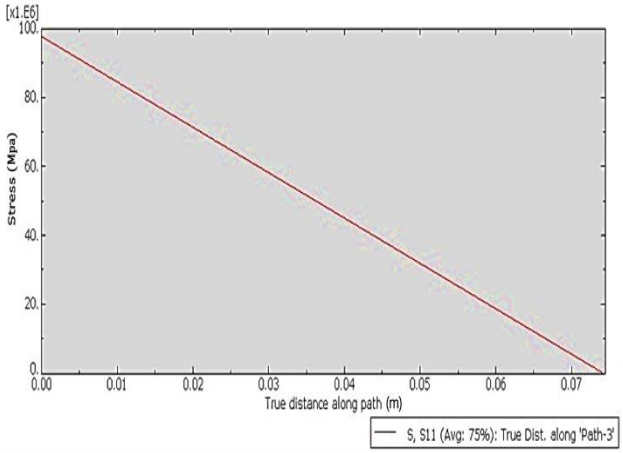

Figure 22. Longitudinal residual stress diagram in a path of the workpiece

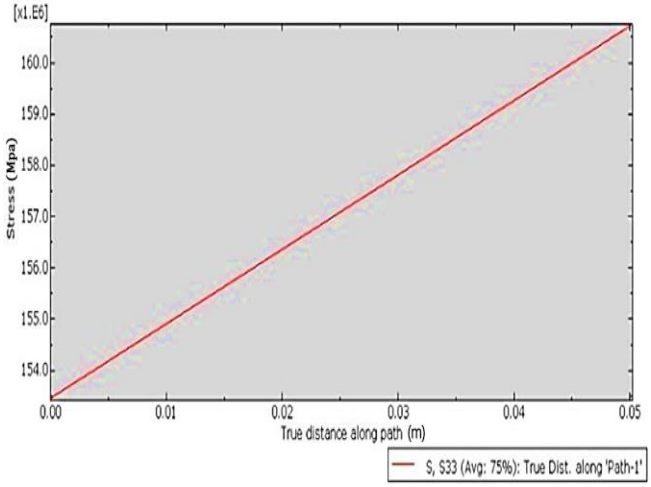

Figure 23. Transverse residual stress diagram in a path of the workpiece

Figure 24 shows the diagram of longitudinal residual stress in a path of the part simulated in this research. Figure 25 also shows the longitudinal residual stress in one path of the part by the sample model [33]. The comparison of these two graphs shows that there is a good agreement between the simulation results in this research and the sample model [33] despite the aluminum alloy not being the same. It can also be seen that both models follow a similar pattern in the change of residual stress in the middle and sides of the workpiece. Figure 26 shows the distortion diagram of the piece in the y direction and Figure 27 also shows the maximum stress diagram at a point of the welding path, simulated in this research.

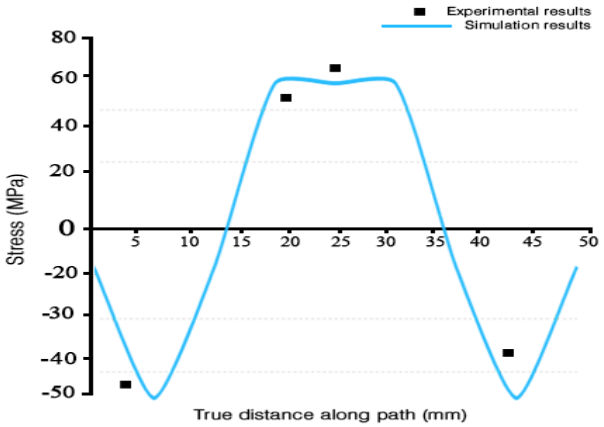

Figure 24. Longitudinal residual stress diagram of a path of the piece in numerical simulation

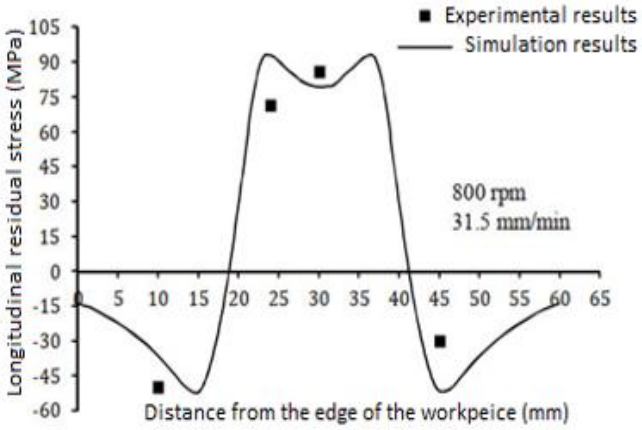

Figure 25. Longitudinal residual stress diagram of a sample model [33]

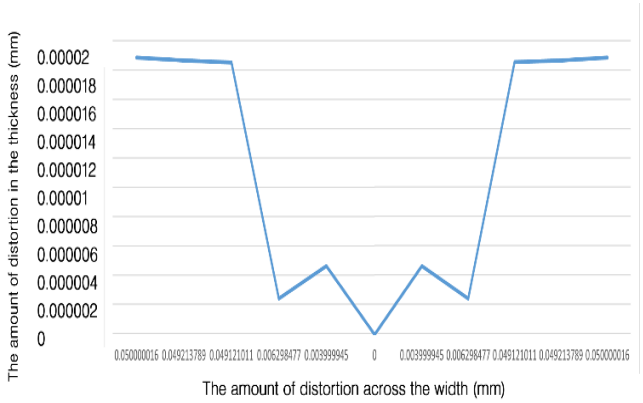

Figure 26. Work piece distortion diagram in y direction

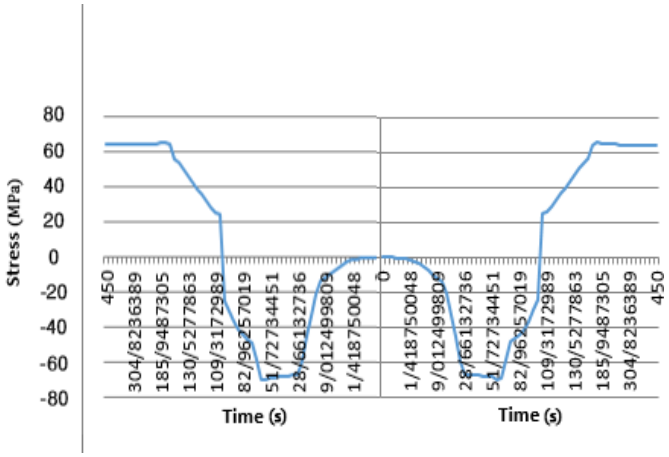

Figure 27. Diagram of the maximum stress at a point of the welding path

4. Conclusion

Temperature prediction leads to the assessment of the state of stresses, strains, and material flow during the FSW. So this research aims to find out the thermal and mechanical properties of AA6063-T5 in the FSW by carrying out thermal and mechanical, simulations.

- To investigate the thermal and mechanical condition of AA6063-T5, in FSW, two simulation steps were performed using Abaqus Standard 2022 software. The first simulation was done using the Fortran coding method in the form of a DFLUX subroutine to check the temperature distribution in this alloy. Then, using the output of the first simulation, the second simulation was performed to check the resulting stresses in this process.
- By comparing the results of numerical simulations of longitudinal residual stresses with the experimental results, the results indicate proper agreement. Therefore, numerical simulation by thermal method can be used as a suitable method for predicting residual stress in FSW.
- A comparison of the simulation results of this research with experimental samples indicates that thermal numerical simulation can be used as a suitable method for predicting stresses and strains and other mechanical properties in FSW.
- If the aim of the research is only to investigate the residual stresses, it is better to consider the length and width of the workpiece to be larger, so that the way of heat distribution in the piece can

be done on a larger level. In other words, the applied heat flux is introduced to points far from the weld metal, as a result, the heat-affected zone in the AA6063-T5, and the resulting tensions are still close to the real results.

6. References

[1] Rabiezadeh, A. and Afsari A. 2019. Effect of nanoparticles addition on dissimilar joining of aluminum alloys by friction stir welding. Journal of Welding Science and Technology of Iran. 4(2):23-34.

[2] Afsari, A., Heidari, S. and Jafari, J. 2020. Evaluation of optimal conditions, microstructure, and mechanical properties of aluminum to copper joints welded by FSW. Journal of Modern Processes in Manufacturing and Production, 9(4):61-81. dor: 20.1001.1.27170314.2020.9.4.6.4.

[3] Li, K., Jarrar, F., Sheikh-Ahmad, J. and Ozturk, F. 2017. Using coupled Eulerian Lagrangian formulation for accurate modeling of the friction stir welding process. Procedia Engineering. 207: 574-579. doi:10.1016/j.proeng.2017.10.1023.

[4] Niazi, M., Afsari, A., Behgozin, A. and Nazemosadat, M. R. 2023. Multi-objective optimization of kinematic tool parameters in FSW of Al-7075 and Al-6061 alloys by RSM. Journal of Welding Science and Technology of Iran. 9(1): 17-29. doi: 10.47176/JWSTI.2023.02.

[5] Buchibabu, V., Reddy, G. M., Kulkarni, D. and De, A. 2016. Friction stir welding of a thick Al-Zn-Mg alloy plate. Journal of Materials Engineering and Performance. 25:1163-1171. doi:10.1007/s11665-016-1924-8.

[6] Ahmed, S., Rahman, R. A. U., Awan, A., Ahmad, S., Akram, W., Amjad, M., Rahimian Koloor and S. S. 2022. Optimization of process parameters in friction stir welding of Aluminum 5451 in marine applications. Journal of Marine Science and Engineering. 10(10):1539. doi: 10.3390/jmse10101539.

[7] Chandrashekar, A., Kumar, B. A. and Reddappa, H. N. 2015. Friction stir welding: tool material and geometry. AKGEC International Journal of Technology. 6(1): 16-20.

[8] Meilinger, A. and Török, I. 2013. The importance of friction stir welding tool. Production Processes and Systems. 6(1): 25-34.

[9] Sambasivam, S., Gupta, N., Singh, D. P., Kumar, S., Giri, J. M. and Gupta, M. 2023. A review paper of FSW on dissimilar materials using aluminum. Materials Today: Proceedings. doi: 10.1016/j.matpr.2023.03.304.

[10] Aziz, S. B., Dewan, M. W., Huggett, D. J., Wahab, M. A. and Okeil, A. M., Liao, T. W. 2018. A fully coupled thermomechanical model of friction stir welding (FSW) and numerical studies on process parameters of lightweight aluminum alloy joints. Acta Metallurgica Sinica (English Letters). 31:1-18. doi: 10.1007/s40195-017-0658-4.

[11] Dialami, N., Cervera, M. and Chiumenti, M. 2018. Effect of the tool tilt angle on the heat generation and the material flow in friction stir welding. Metals. 9(1):28. doi: 10.3390/met9010.

[12] Derazkola, H. A., Kordani, N. and Derazkola, H. A. 2021. Effects of friction stir welding tool tilt angle on properties of Al-Mg-Si alloy T-joint. CIRP Journal of Manufacturing Science and Technology. 33:264-276. doi: 10.1016/j.cirpj.2021.03.015.

[13] Meyghani, B. and Awang, M. 2022. The influence of the tool tilt angle on the heat generation and the material behavior in friction stir welding (FSW). Metals. 12(11):1837. doi: 10.21203/rs.3.rs-1984818/v1.

[14] Ghiasvand, A. and Hassanifard, S. 2018. Numerical simulation of FSW and FSSW with pinless tool of AA6061-T6 Al alloy by CEL approach. Journal of Solid and Fluid Mechanics. 8(3):65-75. doi: 10.22044/jsfm.2018.6522.2528.

[15] Chupradit, S., Bokov, D. O., Suksatan, W., Landowski, M., Fydrych, D., Abdullah, M. E. and Derazkola, H. A. 2021. Pin angle thermal effects on friction stir welding of AA5058 aluminum alloy: CFD simulation and experimental validation. Materials. 14(24):7565. doi: 10.3390/ma14247565.

[16] Ghiasvand, A., Kazemi, M., Mahdipour Jalilian, M. and Ahmadi Rashid, H. 2020. Effects of tool offset, pin offset, and alloys position on maximum temperature in dissimilar FSW of AA6061 and AA5086. International Journal of Mechanical and Materials Engineering. 15:1-14. doi: 10.1186/s40712-020-00118-y.

[17] Derazkola, H. A. and Simchi, A. 2018. Experimental and thermomechanical analysis of the effect of tool pin profile on the friction stir welding of poly (methyl methacrylate) sheets. Journal of Manufacturing Processes. 34:412-423. doi: 10.1080/13621718.2017.1364896.

[18] Shojaeefard, M. H., Akbari, M., Asadi, P. and Khalkhali, A. 2017. The effect of reinforcement type on the microstructure, mechanical properties, and wear resistance of A356 matrix composites produced by FSP. The International Journal of Advanced Manufacturing Technology. 91:1391-1407. doi: 10.1007/s00170-016-9853-0.

[19] Shojaeefard, M. H., Akbari, M., Khalkhali, A., Asadi, P. 2018. Effect of tool pin profile on distribution of reinforcement particles during friction stir processing of B4C/aluminum composites. Proceedings of the Institution of Mechanical Engineers, Part L: Journal of Materials: Design and Applications. 232(8):637-651. doi: 10.1177/1464420716642471.

[20] Akbari, M., Rahimi Asiabaraki, H., Hassanzadeh, E. and Esfandiar, M. 2023. Simulation of dissimilar friction stir welding of AA7075 and AA5083 aluminium alloys using Coupled Eulerian–Lagrangian approach. Welding International. 37(4):174-184. doi: 10.1080/09507116.2023.2205035.

[21] Akbari, M., Asiabaraki, H. R. and Aliha, M. R. M. 2023. Investigation of the effect of welding and rotational speed on strain and temperature during friction stir welding of AA5083 and AA7075 using the CEL approach. Engineering Research Express. 5(2):025012. doi: 10.1088/2631-8695/acca00.

[22] El-Sayed, M. M., Shash, A. Y., Abd-Rabou, M. and ElSherbiny, M. G. 2021. Welding and processing of metallic materials by using friction stir technique: A review. Journal of Advanced Joining Processes. 3:100059. doi: 10.1016/j.jajp.2021.100059.

[23] Meyghani, B. and Wu, C. 2020. Progress in thermomechanical analysis of friction stir welding. Chinese Journal of Mechanical Engineering. 33:1-33. doi: 10.1186/s10033-020-0434-7.

[24] Lemi, M., Gutema, E. and Gopal, M. 2022. Modeling and simulation of friction stir welding process for AA6061-T6 aluminum alloy using finite element method. Engineering Solid Mechanics. 10(2):139-152. doi: 10.5267/j.esm.2022.2.001.

[25] Mishin, V., Shishov, I., Kalinenko, A., Vysotskii, I., Zuiko, I., Malopheyev, S. and Kaibyshev, R. 2022. Numerical simulation of the thermo-mechanical behavior of 6061 aluminum alloy during friction-stir welding. Journal of Manufacturing and Materials Processing. 6(4):68. doi: 10.3390/jmmp6040068.

[26] Xiao, Y. and Wu, H. 2020. An explicit coupled method of FEM and meshless particle method for simulating transient heat transfer process of friction stir welding. Mathematical Problems in Engineering. 2020:1-16. doi:10.1155/2020/2574127.

[27] Akbari, M., Asadi, P. and Sadowski, T. 2023. A review on friction stir welding/processing: numerical modeling. Materials. 16(17):5890. doi: 10.3390/ma16175890.

[28] Soori, M. Asmael, M and Solyalı, D. 2021. Recent development in friction stir welding process. SAE. International Journal of Materials and Manufacturing. 14(1):63-80. doi: 10.4271/05-14-01-0006.

[29] Ji, S. D., Jin, Y. Y., Yue, Y. M., Gao, S. S., Huang, Y. X. and Wang, L. 2013. Effect of temperature on material transfer behavior at different stages of friction stir welded 7075-T6 aluminum alloy. Journal of Materials Science & Technology. 29(10):955-960. doi: 10.1016/j.jmst.2013.05.018.

[30] Schmidt, H., Hattel, J. and Wert, J. 2003. An analytical model for the heat generation in friction stir welding. Modelling and Simulation in Materials Science and Engineering. 12(1):143. doi: 10.1088/0965-0393/12/1/013.

[31] Gholami, N., Afsari, A., Nazemosadat, S. M. R. and Afsari, M. J. 2023. Simulation and dynamic-thermal analysis of ceramic disc and brake pad for optimization by finite element method. International Journal of Advanced Design & Manufacturing Technology. 16(4):9-22. doi: 10.30486/admt.2024.1980467.1402.

[32] Nazemosadat, S. M. R., Ghanbarian, D., Naderi-Boldaji, M. and Nematollahi, M. A. 2022. Structural analysis of a mounted moldboard plow using the finite element simulation method. Spanish Journal of Agricultural Research. 20(2):e0204-e0204. doi: 10.5424/sjar/2022202-18157.

[33] Ghahremani Moghadam, D., Farhang Doost, K., Rastegar, A. and Ramezani Moghaddam, M. 2015. Tool's Speed effect on hardness and residual stress in friction stir welded Al 2024-T351: Experimental method and Numerical simulation. Modares Mechanical Engineering. 15(2):61-71. doi: 20.1001.1.10275940.1394.15.2.18.6.